Chiral Induction by Seeding Surface Assemblies of Chiral Switches

8 AUTHORS, INCLUDING:

Chiral Induction by Seeding Surface Assemblies of Chiral Switches

Federico Masini,[‡] Nataliya Kalashnyk,[‡] Martin M. Knudsen,[§] Jacob R. Cramer,[§] Erik Lægsgaard,[‡] Flemming Besenbacher,[‡] Kurt V. Gothelf,*[,§] and Trolle R. Linderoth*[,‡]

[‡]Sino-Danish Center for Molecular Nanostructures on Surfaces, Interdisciplinary Nanoscience Center (iNANO), and Department of Physics and Astronomy, Aarhus University, Ny Munkegade 118, 8000 Aarhus C, Denmark

[§]Sino-Danish Center for Molecular Nanostructures on Surfaces, Interdisciplinary Nanoscience Center (iNANO) and Department of Chemistry, Aarhus University, Langelandsgade 140, 8000 Aarhus C, Denmark

ABSTRACT: It is demonstrated by scanning tunneling microscopy that coadsorption of a molecular chiral switch with a complementary, intrinsically chiral induction seed on the Au(111) surface leads to the formation of globally homochiral molecular assemblies.

Developing efficient ways to form chiral surfaces by functionalization with molecules is technologically highly relevant, e.g., within areas such as asymmetric heterogeneous catalysis[1] or chiral separation and chromatography.[2] Understanding how molecular chirality is transferred and amplified at surfaces may also help elucidate the fundamental origins of biomolecular homochirality.[3] Local-probe scanning tunneling microscopy (STM) has been demonstrated to directly reveal molecular and supramolecular chirality and give unprecedented insights in chiral molecular adsorption on surfaces.[4−7] Deposition of racemic mixtures on surfaces often leads to formation of two-dimensional conglomerates, i.e., the molecules segregate into locally homochiral domains while the surface remains globally racemic.[8] The situation is similar for prochiral compounds, which are intrinsically achiral, but become chiral upon adsorption owing to reduction of symmetry or confinement of particular conformational states, always leading to equal amounts of opposite surface enantiomers.[9−11] Globally homochiral surfaces are most obviously achieved by deposition of enantiomerically pure compounds.[12] An interesting alternative is chiral induction where the chirality is steered toward one specific handedness,[13−15] e.g., by an external agent[16,17] or by the "majority rule" where an enantiomeric excess is amplified in the resulting supramolecular structures.[18,19]

In the "sergeants and soldiers" approach to chiral induction,[20] a homochiral seed induces a chiral response in target molecules. This has been elegantly demonstrated in surface assemblies using enantiopure tartaric acid (TA) as an induction agent (sergeant) for the structurally related, but achiral succinic acid (soldier),[21] as well as for the achiral meso form of TA.[22] In both these cases, chiral induction was observed by the averaging technique of low-energy electron diffraction while detailed microscopic (STM) observations of the induction process were not obtained (enantiospecific embedding of individual TA molecules in a 2D matrix of succinic acid has been observed by STM, but for a different structural phase[23]). Very recently, chiral induction by coadsorption of enantiopure malic acid with a surface conglomerate formed by racemic TA was reported.[15] For this system, STM observations revealed formation of a semiordered mixture of the induction agent and one of the TA enantiomers, while

ordered domains formed by the opposite TA enantiomer persisted, i.e., the induction agent served to destroy rather than seed chirally ordered structures. In general, however, there is a need to expand investigation of chiral induction by seeding to other molecular systems, and to improve the microscopic understanding of basic mechanisms underlying chiral induction.

Here, we use high-resolution STM to directly reveal chiral induction at surfaces in a two-component system, consisting of a conformational chiral molecular switch and a complementary, custom-designed chiral induction seed. We investigate two different protocols toward chiral induction, termed nucleation and intermixing, and from careful statistical analysis, we demonstrate the latter to be superior since it suppresses nucleation of domains with unbiased chirality.

The molecular model system is shown in Scheme 1 and consists of a linear molecular rod formed from an oligo(phenylene-ethynylene) (OPE) backbone functionalized at both ends with bulky alkyl substituents. In the achiral compound **1**, the alkyl substituents are *tert*-butyl groups, whereas in the homochiral compound **S-2**, chiral (*S*)-*sec*-butyl groups are used. We have previously reported on the chemical synthesis of these compounds, and by means of STM studies, we have revealed the adsorption patterns formed by the individual compounds on the Au(111) surface under ultrahigh vacuum (UHV) conditions.[24−27] Compound **1** is prochiral and displays conformational chirality in the sense that it can adsorb in different conformations distinguished by the positions (left/right) of the *tert*-butyl groups with respect to the molecular backbone, two of which (RR and LL) are chiral enantiomers (Scheme 1b). Compound **1** is a chiral switch since it can undergo conformational changes involving rotation of the terminal groups around the molecular axis even after adsorption on the surface, allowing it to switch between the R and L orientations. The compound forms an adsorption structure with a pronounced chiral organization of the molecular backbones based on a windmill motif which can assume either a clockwise or counterclockwise sense of rotation. In this structure, organizational and conformational chirality are correlated by the requirement that the *tert*-butyl pendants are placed at the outside of the windmill nodes (Scheme 1c). Since **1** is prochiral, the two conformational surface enantiomers and the associated mirror-image windmill domains are always formed in equal amounts.[24] The intrinsically chiral compound **S-2** forms windmill assemblies which are structurally very similar to those obtained for **1**, but the subtle change in molecular design very importantly results in a

Scheme 1[a]
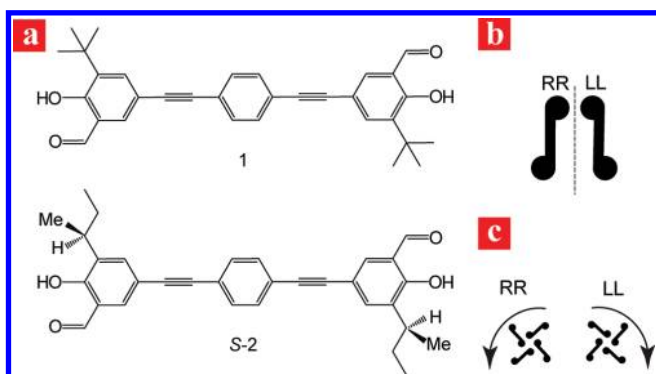
[a] (a) Molecular model system based on rod-shaped molecules with oligo(phenylene ethynylene) (OPE) backbones and salicylaldehyde terminal groups. For the prochiral molecule **1**, the end groups contain *tert*-butyl groups while the intrisically chiral molecule **S-2** contains two chiral (*S*)-*sec*-butyl groups. (b) Schematic representation of conformations assumed after adsorption. Black circles represent the *tert*-butyl or (*S*)-*sec*-butyl groups, while the black rods represent the OPE molecular backbone. The R and L (right and left) nomenclature refers to the position of the two *tert/sec*-butyl groups with respect to the molecular backbone when observing it from the central benzene ring. For **1**, the RR and LL conformations constitute mirror image surface enantiomers. (c) Schematic representation of windmill motifs formed by molecules in RR and LL conformation, respectively.

strong preference for the RR conformational state and windmill domains with the associated sense of rotation (see ref 27). The structural similarity between **1** and **S-2**, the similarity of the patterns they form on Au(111), and the ability of **1** to switch surface chirality make the molecules ideal for investigation of chiral communication between the molecules and for seeding of structures formed by the achiral compound **1** with enantiopure **S-2**.

The experiments to codeposit the two molecules on a Au(111) surface were performed in an UHV system with a base pressure in the low 10^{-10} mbar regime and equipped with a home-built variable temperature Aarhus STM.[28] The Au(111) single crystal was cleaned by several cycles of 1.5 keV Ar^+ sputtering followed by annealing at 850 K, resulting in an atomically clean $(22 \times \sqrt{3})$ herringbone reconstructed Au(111) surface. The molecules were sublimated from separate, resistively heated glass crucibles maintained at 378 K (**S-2**) and 393 K (**1**) and held within a few centimeters from the Au surface. Typical dosing times were 1.5–3 min resulting in submonolayer coverage. STM images were acquired in the temperature range 120–130 K.

In the "nucleation protocol" toward chiral induction, **S-2** molecules were first deposited onto a Au(111) surface held at 300 K. Then, the sample was slowly (6 K/min) cooled to 200 K in order to allow formation of ordered **S-2** islands. Subsequently, the prochiral molecules **1** were dosed onto this surface at 200 K and the surface was maintained at this temperature for a 30 min postdeposition annealing. This annealing temperature was chosen since it was expected to be sufficiently high to allow the chiral switches **1** to diffuse and accommodate to the islands formed from **S-2** while being low enough that the preformed **S-2** islands were thermally stable. The sample was subsequently cooled to 120K (6 K/min) and imaged with STM.

In Figure 1a is depicted an STM image of the interior of a molecular island resulting from this nucleation protocol. It has
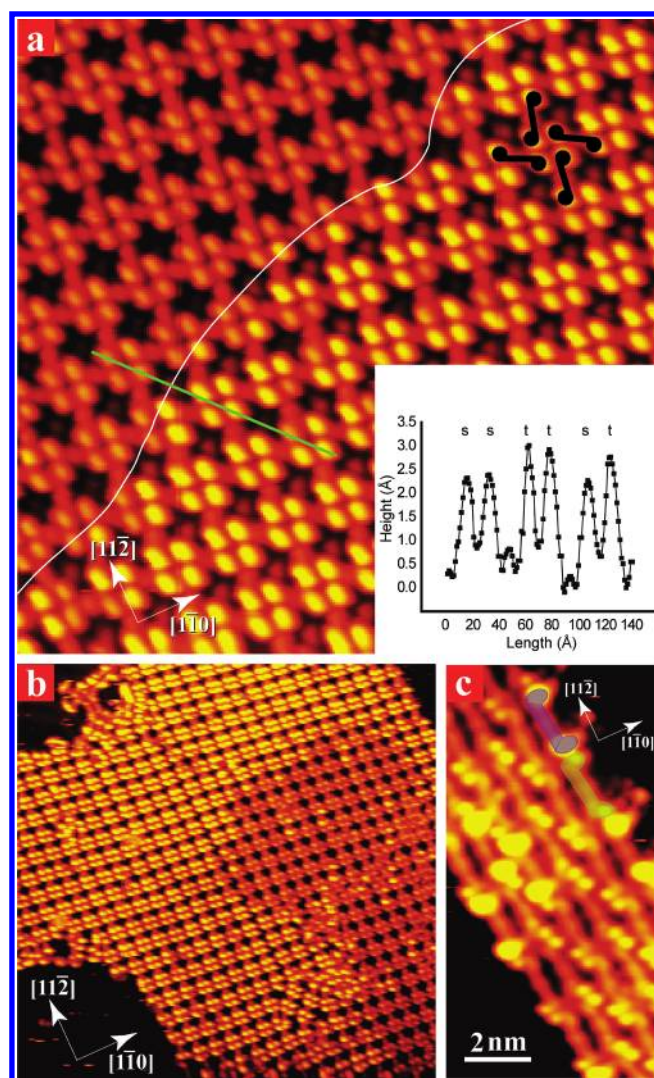

Figure 1. Chiral induction by the nucleation protocol. (a) STM image showing the interior of a nucleation induced windmill island on the Au(111) surface (259 Å × 257 Å; $I = -0.4$ nA; $V = -2.09$ V). A schematic model of the windmill motif formed from molecules in RR conformation is indicated. Bright/dim protrusions correspond to *tert*-butyl/*sec*-butyl groups and the white line indicates the boundary between homomolecular regions formed from **S-2** (upper left) and **1** (lower right). Inset: Height profile acquired along the line shown in green; *s* and *t* above the peaks indicate *sec* and *tert*-butyl groups, respectively. (b) Larger scale image of nucleation induced island (604 Å × 599 Å; $I = -0.55$ nA; $V = -2.09$ V). (c) STM image of a brick-wall molecular island formed after codeposition of **1** and **S-2** on Au(111). (64 Å × 125 Å; $I = -0.41$ nA; $V = -2.02$ V). Brick-wall islands with parallel stacking of the molecular backbones were previously observed to coexist with windmill islands for both **1** and **S-2**. In the case of **S-2**, the structure consists entirely of molecules in RL conformation, organized such that the *sec*-butyl groups on two neighboring molecules are always placed on the same side of the molecular rows where two molecules meet end-to-end.[27] In marked contrast, the brick-wall phase formed from **1** is conformationally disordered with RR, LL, and RL conformations participating.[25] In the co-deposition experiments, brick-wall islands were occasionally observed, but constitute a clear minority. The shown mixed brick-wall island both contains molecules with dim and bright protrusions. The molecules with dim protrusions are conformationally ordered and correspond to the structure in brick-wall islands formed from **S-2**, allowing unambiguous assignment of the two species.

the windmill structure observed previously for both **1** and **S-2**, in this case exhibiting windmill motifs with a counter-clockwise sense of rotation corresponding to molecules in RR conformation (compare overlay of schematic molecular models). The characteristic protrusions associated with the alkyl side pendants display two different brightness levels, corresponding to a ~0.5 Å difference in their apparent height, as revealed by the STM height profile shown in the inset (acquired along the green line indicated in the STM image). One molecule in the structure always has either dim or bright protrusions associated with it, and we therefore attribute the contrast difference to the nature of the side pendant (*sec*-butyl or *tert*-butyl), conveniently allowing **1** and **S-2** to be distinguished in the STM image. Absolute assignment of the brightest protrusions to the *tert*-butyl groups of **1** and the dimmer protrusions to the *sec*-butyl groups of **S-2** is possible based on observations of a coexisting brickwall structure shown in Figure 1c (see caption of Figure 1 for details). In the windmill island of Figure 1a, the upper left region is thus dominated by **S-2**, while the lower right-hand region is dominated by **1**. A larger-scale image of an induced windmill island is shown in Figure 1b, clearly revealing a core region formed from the intrinsically chiral **S-2** molecules surrounded by a rim formed from **1**. Occasional examples of individual **S-2** molecules embedded in the regions of **1** and vice versa are also observed, showing a slight intermixing during or after deposition of **1**. The boundary between the two homomolecular regions, indicated by a white line in Figure 1a, is continuous, and the two windmill structures therefore adapt well to each other, allowing for specific interactions between the two types of molecules. Growth of **1** from nuclei formed from **S-2** therefore appears to have occurred, and the conformation/chiral arrangement in the regions formed from the chiral switches **1** match that in the regions of the intrinsically chiral compound **S-2**, demonstrating a local chiral induction effect between the nucleus and the surrounding growth region.

To establish if chiral induction occurred globally on the surface, a thorough statistical analysis was performed based on five identical sample preparations. Here, we systematically surveyed a total of 19 sample areas (nominally of $2 \times 2 \ \mu m^2$ extension as accessible by the STM scanner head) and recorded STM images of the encountered islands. Of 44 observed islands showing a clear boundary between regions formed from **S-2** and **1** (nucleation induced windmill islands), 96% were of the RR conformation with a counterclockwise arrangement of the windmill motifs, while only 4% were of the LL conformation. This matches well the bias for RR over LL observed in experiments with pure **S-2**.[27] However, the survey also revealed 36 islands uniquely composed of **1**, ascribed to nucleation occurring in the second step of the preparation protocol during deposition of **1**. Within experimental error, these islands show RR and LL arrangement with equal distribution as anticipated for the prochiral compound **1**. If these islands are included in the statistics, the overall distribution is 70% RR versus 30% LL windmill islands. While there is thus a clear chiral bias globally on the surface, this is to some extent diluted by random nucleation of islands formed entirely by **1**. Attempts to remedy this by creating a higher density of chirally biased nucleation points through control of deposition rate and substrate temperature during the initial deposition of **S-2** were not successful.

To circumvent random nucleation of islands formed entirely from **1**, we devised an alternative "intermixing protocol". Here, both compounds were sequentially dosed onto a Au(111) surface held at room temperature (300 K). Subsequently, the sample
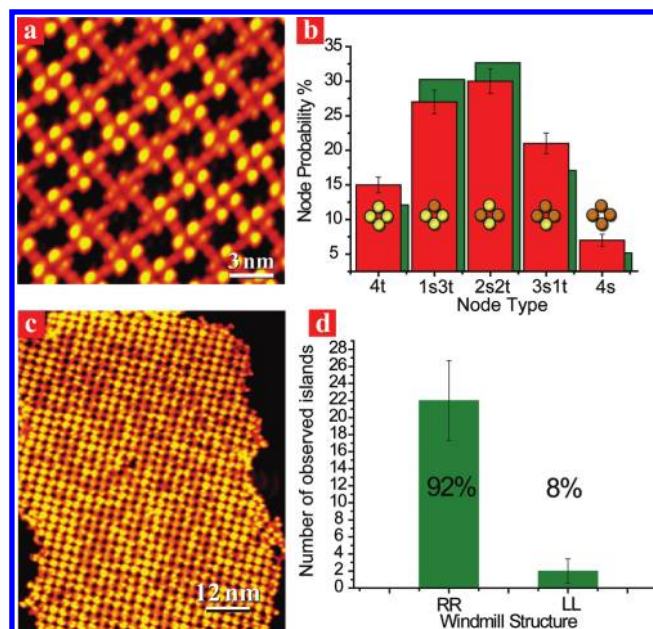

Figure 2. Chiral induction by the intermixing protocol. (a) STM image of intermixing-induced windmill island on the Au(111) surface (171 Å × 173 Å; $I = -0.37$ nA; $V = -1.25$ V). (b) Histogram (red) showing the observed distribution of bright *tert* (*t*) and dim *sec* (*s*) butyl groups in the nodes of the windmill structure. A binomial distribution (green) corresponding to the observed probabilities $P(s) = 0.42$ and $P(t) = 0.58$ is shown for comparison (the distribution is asymmetric due to the different fractions of **S-2** and **1**) . (c) Large-scale STM image of an intermixed island (701 Å × 846 Å; $I = -0.48$ nA; $V = -1.25$ V). (d) Histogram showing the distribution of observed windmill domains after the intermixing protocol; a clear preference for the RR windmill structure is observed.

was annealed at 320 K for 30 min after which it was slowly cooled (6 K/min) to 120 K. The intermediate annealing step was introduced in order to allow thermal dissociation of existing islands and intermixing of the two species by diffusion.

Figure 2a shows the interior of an RR windmill island resulting from this growth protocol. Again, two different species can clearly be discerned based on the apparent STM height of the peripheral groups, but in contrast to the situation in Figure 1b, they are now indeed thoroughly intermixed. Systematic survey of the surface following the intermixing protocol shows that extended structures consisting entirely of **S-2** or **1** are not formed. (Interestingly, formation of brick-wall phases appears also to be suppressed as areas with this structure were only observed to a negligible extent). To quantify the degree of intermixing of the two species, we analyzed the island shown in Figure 2c with respect to the distribution of *sec*-butyl (*s*) and *tert*-butyl (*t*) groups in the individual windmill nodes where four molecules join to form the structure. In Figure 2b is depicted a histogram (red) obtained from analysis of 865 nodes, showing that all node combinations are realized, as may also be observed in the high-resolution STM image of Figure 2a. For comparison, a binomial distribution for the probabilities $P(s) = 0.42$ and $P(t) = 0.58$, corresponding to the respective fractions of **S-2** and **1** in the analyzed island, is shown in green. The good correspondence between the two distributions demonstrates a near-random intermixing of the two species, possibly with a slight bias toward the homomolecular 4*s* and 4*t* nodes.

Figure 2d shows the distribution between RR and LL windmill islands resulting from a systematic survey of the surface following the intermixing protocol. There is in this case a clear preference for islands with RR chirality, thereby demonstrating that the intermixing protocol indeed leads to chiral induction globally on the surface. This result is enabled by the ability of the achiral target molecules **1** to switch surface conformation/chirality and adapt to the conformation preferred by the structurally similar chiral seeding molecules **S-2** in combination with an induction protocol ensuring that all target molecules participate in domains affected by the seeds. The very small fraction of LL domains contain **S-2** molecules in the unpreferred LL conformation, similar to the situation for pure **S-2** (ref 27). Their presence is ascribed to a sufficiently low energy difference between the LL and RR conformations for **S-2** to allow a small population of the minority conformer. Further experiments will be required to establish/optimize the minimum fraction of **S-2** molecules necessary to maintain a global induction effect by the intermixing protocol.

In the previously investigated tartaric/succinic acid system, chiral induction was also attributed to a bistable target molecule, in this case resulting from two mirror-image adsorption geometries, but direct-space, microscopic details of the mechanism for the chiral amplification/ordering process were not provided.[13,21] In contrast to the situation for enantiopure malic acid coadsorbed with a surface conglomerate formed by racemic TA, for which STM results were recently reported upon,[15] the chiral seeds in the present case participate in the ordered chiral structure formed, and there is not a significant portion of the surface covered by disordered regions of the suppressed enantiomer.

In conclusion, it was demonstrated that a globally homochiral molecular structure was achieved based on chiral induction between intrinsically chiral molecular "sergeants" (**S-2**) and prochiral "soldiers" in the form of chiral switches (**1**). We demonstrate that careful engineering and synthesis of a chiral seed, capable of interacting with a structurally similar target molecule through chiral recognition, can be utilized to steer surface chirality toward global homochirality: The present findings thus opens interesting perspectives for efficient chiral surface functionalization which may have applications in asymmetric heterogeneous catalysis, chiral separation and chromatography.

■ AUTHOR INFORMATION

Corresponding Author
kvg@chem.au.dk, trolle@inano.au.dk

■ REFERENCES

(1) Mallat, T.; Orglmeister, E.; Baiker, A. *Chem. Rev.* **2007**, *107*, 4863–4890.
(2) Lammerhofer, M.; Gargano, A. *J. Pharm. Biomed. Anal.* **2010**, *53*, 1091–1123.
(3) Hazen, R. M.; Sholl, D. S. *Nat. Mater.* **2003**, *2*, 367.
(4) Raval, R. *Chem. Soc. Rev.* **2009**, *38*, 707–721.
(5) Elemans, J.; De Cat, I.; Xu, H.; De Feyter, S. *Chem. Soc. Rev.* **2009**, *38*, 722–736.
(6) Ernst, K. H. *Top. Curr. Chem.* **2006**, *265*, 209–252.
(7) Gellman, A. J. *ACS Nano* **2010**, *4*, 5–10.
(8) Stevens, F.; Dyer, D. J.; Walba, D. M. *Angew. Chem., Int. Ed. Engl.* **1996**, *35*, 900–901.
(9) Bohringer, M.; Morgenstern, K.; Schneider, W. D.; Berndt, R.; Mauri, F.; De Vita, A.; Car, R. *Phys. Rev. Lett.* **1999**, *83*, 324–327.
(10) Weckesser, J.; De Vita, A.; Barth, J. V.; Cai, C.; Kern, K. *Phys. Rev. Lett.* **2001**, *87*, 096–101.
(11) Chen, Q.; Richardson, N. V. *Nat. Mater.* **2003**, *2*, 324–328.
(12) Ortega Lorenzo, M.; Baddeley, C. J.; Muryn, C.; Raval, R. *Nature* **2000**, *404*, 376–379.
(13) Ernst, K.-H. *Curr. Opin. Colloid Interface Sci.* **2008**, *13*, 54–59.
(14) Palmans, A. R. A.; Meijer, E. W. *Angew. Chem., Int. Ed.* **2007**, *46*, 8948–8968.
(15) Roth, C.; Passerone, D.; Ernst, K.-H. *Chem. Commun.* **2010**, *46*, 8645–8647.
(16) Katsonis, N.; Xu, H.; Haak, R. M.; Kudernac, T.; Tomovic, Z.; George, S.; Van der Auweraer, M.; Schenning, A.; Meijer, E. W.; Feringa, B. L.; De Feyter, S. *Angew. Chem., Int. Ed.* **2008**, *47*, 4997–5001.
(17) Berg, A. M.; Patrick, D. L. *Angew. Chem., Int. Ed.* **2005**, *44*, 1821–1823.
(18) Fasel, R.; Parschau, M.; Ernst, K.-H. *Nature* **2006**, *439*, 449.
(19) Haq, S.; Liu, N.; Humblot, V.; Jansen, A. P. J.; Raval, R. *Nat. Chem.* **2009**, *1*, 409–414.
(20) Green, M. M.; Reidy, M. P.; Johnson, R. J.; Darling, G.; Oleary, D. J.; Willson, G. *J. Am. Chem. Soc.* **1989**, *111*, 6452–6454.
(21) Parschau, M.; Romer, S.; Ernst, K.-H. *J. Am. Chem. Soc.* **2004**, *126*, 15368.
(22) Parschau, M.; Kampen, T.; Ernst, K. H. *Chem. Phys. Lett.* **2005**, *407*, 433–437.
(23) Liu, N.; Haq, S.; Darling, G. R.; Raval, R. *Angew. Chem., Int. Ed.* **2007**, *46*, 7613–7616.
(24) Weigelt, S.; Busse, C.; Petersen, L.; Rauls, E.; Hammer, B.; Gothelf, K. V.; Besenbacher, F.; Linderoth, T. R. *Nat. Mater.* **2006**, *5*, 112–117.
(25) Busse, C.; Weigelt, S.; Petersen, L.; Lægsgaard, E.; Besenbacher, F.; Linderoth, T. R.; Thomsen, A. H.; Nielsen, M.; Gothelf, K. V. *J. Phys. Chem. B* **2007**, *111*, 5850–5860.
(26) Bombis, C.; Weigelt, S.; Knudsen, M. M.; Nårgaard, M.; Busse, C.; Lagsgaard, E.; Besenbacher, F.; Gothelf, K. V.; Linderoth, T. R. *ACS Nano* **2010**, *4*, 297–311.
(27) Knudsen, M. M.; Kalashnyk, N.; Masini, F.; Cramer, J. R.; Lægsgaard, E.; Besenbacher, F.; Linderoth, T. R.; Gothelf, K. V. *J. Am. Chem. Soc.* **2011**, *133*, 4896–4905.
(28) Besenbacher, F.; Lægsgaard, E.; Mortensen, K.; Nielsen, U.; Stensgaard, I. *Rev. Sci. Instrum.* **1988**, *59*, 1035–1038.